Remote Sensing

Article

Long-Term Satellite Detection of Post-Fire Vegetation Trends in Boreal Forests of China

Kunpeng Yi [1],*, Hiroshi Tani [2], Jiquan Zhang [3], Meng Guo [4], Xiufeng Wang [2] and Guosheng Zhong [1]

[1] Graduate School of Agriculture, Hokkaido University, Sapporo, Hokkaido 060-8589, Japan;
     E-Mail: zhgs@env.agr.hokudai.ac.jp

[2] Research Faculty of Agriculture, Hokkaido University, Sapporo, Hokkaido 060-8589, Japan;
     E-Mails: tani@env.agr.hokudai.ac.jp (H.T.); wang@env.agr.hokudai.ac.jp (X.W.)

[3] School of Environmental Sciences, Northeast Normal University, Changchun 130117, China;
     E-Mail: zhangjq022@nenu.edu.cn

[4] School of Geographical Sciences, Northeast Normal University, Changchun 130024, China;
     E-Mail: guomeng1981@gmail.com

* Author to whom correspondence should be addressed; E-Mail: yikp@env.agr.hokudai.ac.jp;
    Tel.: +81-011-706-3569; Fax: +81-011-706-2494.

Abstract: This paper describes the long-term effects on vegetation following the catastrophic fire in 1987 on the northern Great Xing'an Mountain by analyzing the AVHRR GIMMS 15-day composite normalized difference vegetation index (NDVI) dataset. Both temporal and spatial characteristics were analyzed for natural regeneration and tree planting scenarios from 1984 to 2006. Regressing post-fire NDVI values on the pre-fire values helped identify the NDVI for burnt pixels in vegetation stands. Stand differences in fire damage were classified into five levels: Very High (VH), High (H), Moderate (M), Low (L) and Slight (S). Furthermore, intra-annual and inter-annual post-fire vegetation recovery trajectories were analyzed by deriving a time series of NDVI and relative regrowth index (RRI) values for the entire burned area. Finally, spatial pattern and trend analyses were conducted using the pixel-based post-fire annual stands regrowth index (SRI) with a nonparametric Mann-Kendall (MK) statistics method. The results show that October was a better period compared to other months for distinguishing the post- and pre-fire vegetation conditions using the NDVI signals in boreal forests of China because colored leaves on grasses and shrubs fall down, while the leaves on healthy trees remain green in October. The

MK statistics method is robustly capable of detecting vegetation trends in a relatively long time series. Because tree planting primarily occurred in the severely burned area (approximately equal to the Medium, High and Very High fire damage areas) following the Daxing'anling fire in 1987, the severely burned area exhibited a better recovery trend than the lightly burned regions. Reasonable tree planting can substantially quicken the recovery and shorten the restoration time of the target species. More detailed satellite analyses and field data will be required in the future for a more convincing validation of the results.

Keywords: wildfire; remote sensing; vegetation recovery; Mann-Kendall; Great Xing'an Mountain; boreal forest

1. Introduction

Wildfire is an important process in regulating vegetation succession, plant regeneration, and species composition in boreal forest ecosystems [1–3]. Large areas of the boreal forest zone, which natural fire have shaped over several millennia, are burned annually. Industrial and recreational use of boreal forests and forest fire suppression capabilities have dramatically increased over the past century [4]. Northeast China maintains abundant forest resources, with a forest area of ~47.0 $\times 10^4$ km^2, occupying 31% of China's total forest area [5]. This region stores 1.0–1.5 Pg C and contributes to approximately 24%–31% of the total carbon storage in China [6]. Most carbon is stored in living trees. For thousands of years, wildfires have been the predominant disturbances in this region, which have been strongly modified by humans during the recent half century. Historically, fire regimes in these systems were characterized by frequent, low intensity surface fires mixed with sparse stand-replacing fires over relatively small areas. From 1950 to 1995, the annual average burned area in the northeast region accounted for 55% of the national total [7]. Wildfires play a dominant role in boreal ecosystems, altering the forest succession, biogeochemical cycling and carbon sequestration [8]. During pre-fire periods, forests are believed to be a net carbon sink—a place where carbon is stored (or sequestered). When wood is burned, carbon is emitted in decomposition, and wildfires are believed to represent a globally significant source of terrestrial carbon in the atmosphere. Following a wildfire, more carbon is absorbed in younger trees during the faster regrowth phases and it is transformed to a carbon sink again after fire. Therefore, a better observational base for understanding post-fire vegetation dynamics in the boreal forests will contribute to predicting the effects of the increasing number of wildfires caused by climate change in these ecosystems and subsequently forecasting the future role of boreal forests as a carbon sink or source [9].

Wildfires create profound changes in ecosystems, causing variations in vegetation reflectance, moisture and temperature, which can be detected by means of satellite imagery [10,11]. Fire disturbance causes substantial spectral changes by consuming vegetation, destroying the leaf chlorophyll, exposing soil, charring stems and altering vegetation moisture. These effects of a fire on vegetative ecosystem properties are often defined as burn severity, which is restricted to the loss of organic matter in or on the soil surface, and in this respect represents what BAER assessments term "soil burn severity" [12]. The post-fire re-growth process is of great importance because while fire releases carbon into the

atmosphere, carbon sequestration through post-fire regeneration of plants and woody vegetation may help to reduce the amount of carbon in the atmosphere [13]. Numerous studies have focused on the use of the Normalized Difference Vegetation Index (NDVI) to analyze seasonal and inter-annual vegetation dynamics and trends following wildfire disturbances [14,15]. The NDVI data capture the contrast between red and near-infrared reflectance of vegetation, which signals the abundance and energy absorption of leaf pigments, e.g., chlorophyll.

NDVI can be used as a proxy for the vegetation response to wildfire disturbances because it is well correlated with vegetation regrowth and the fraction of photosynthetically active radiation absorbed by plant canopies and, thus, leaf area and biomass [16]. In the present paper, NDVI derived from and the Advanced Very High-Resolution Radiometer (AVHRR) satellite measurements is exploited to investigate post-fire regeneration and temporal dynamics in the boreal forest. Because of an unusually prolonged drought and high winds in northeastern China, the Great Xing'an Mountains exploded in a catastrophic wildfire in May 1987. The success of fire suppression in this region, coupled with a warmer, drier climate due to global warming, has led to fuel buildup and resulted in fires of greater intensity and extent than those that occurred historically in the region [17]. This fire created a mosaic of burn severities across the landscape and provided an ideal opportunity to study post-fire vegetation patterns in a Chinese boreal forest. The main goals of the present work are (i) to assess the fire damage of the entire fire-affected areas in the Great Xing'an Mountains from the fire event in 1987; (ii) to better understand how vegetation responds to fire disturbances by analyzing intra- and inter-annual variability in satellite observations; and (iii) to characterize the spatial pattern of post-fire vegetation trends under natural regeneration and tree planting scenarios using the AVHRR GIMMS NDVI record over the period 1986–2006.

2. Data and Method

2.1. Study Area

The Great Xing'an Mountain is a typical fire-prone ecosystem in which many species have a recognized ability to regenerate after fire. Historically, fire regimes in this region were characterized by frequent, low intensity surface fires mixed with sparse stand-replacing fires over relatively small areas [18]. The Daxing'anling fire occurred on May 6 and was located on the north slope of Great Xing'an Mountain (52°15'N–53°33'N, 121°51'E–125°05'E) in Northeastern China (Figure 1). It is primarily a hilly, mountainous region ranging from 450–1500 m in elevation. This fire burned more than 1.33 million hectares of forest resulting in the loss of over 200 lives and 50,000 homes. Fires of this magnitude are a major but infrequent disturbance to this landscape, occurring at 100- to 300-year intervals [19]. The Daxing'anling fire produced a strikingly heterogeneous mosaic of burn severities (effects of fire on the ecosystem) and islands of unburned vegetation across the landscape. The spatial extent and heterogeneity induced by this fire provide an ideal opportunity to study the effects of fire size and pattern on post-fire succession. The climate in this region is terrestrial monsoon with long, severe winters (mean January temperature −28.5 °C) and short, mild summers (mean July temperature 17 °C). The precipitation, which peaks in summer, is 420 mm annually and is unevenly distributed throughout the year, *i.e.*, more than 60% occurs between June and August. Vegetation in this region

falls within the cool temperate coniferous forests occurring at the southern extension of the eastern Siberian light coniferous forest [20]. The species composition is relatively simple and the forest covers more than 75% of the study area. The most dominant tree species is larch (*Larix gmelini*), accounting for 80% of the study area, followed by birch (*Betula Platy Plylla*), which covers 10% of the study area. Other species, including pine (*Pinus sylvestris var. mongolica*), spruce (*Picea Kor-aiensis*), two species of aspen (*Populus davidiana*, *Populus suaveolens*), and willow (*Chosenia arbutifolia*) cover approximately 10% of the study area.

Figure 1. Location of the study area.
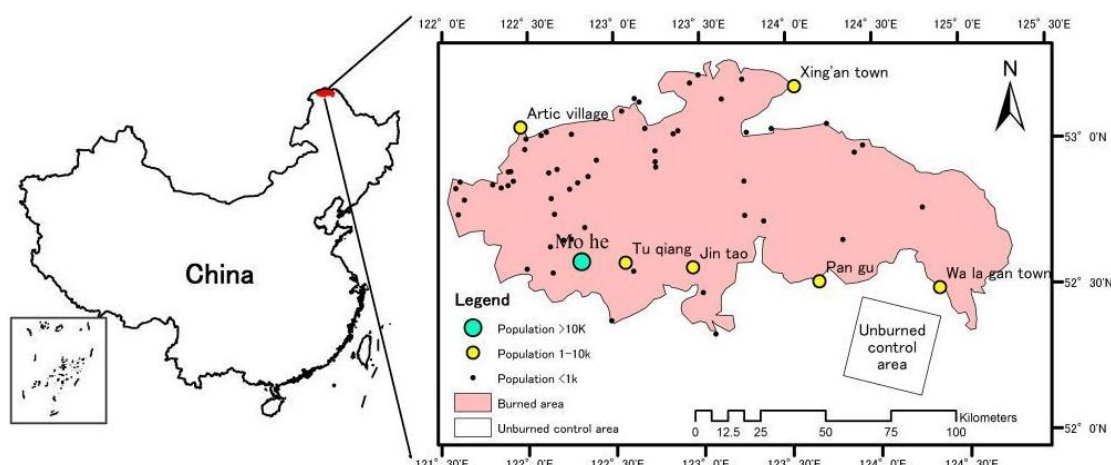
2.2. Data

2.2.1. AVHRR GIMMS 15-Day Composite NDVI Dataset

We used the continental NDVI dataset at 8 km resolution for the period 1984–2006 produced by the Global Inventory Monitoring and Modeling Studies (GIMMS). The dataset was derived from imagery obtained from the AVHRR instrument onboard the NOAA satellite series 7, 9, 11, 14, 16 and 17. It contains channel 1 (0.58–0.68 µm) and channel 2 (0.73–1.1 µm) reflectance, channel 4 (10.3–11.3 µm) and channel 5 (11.5–12.5 µm) brightness temperatures, solar and view zenith angles, and the day of compositing. These channels and associated data correspond to the maximum NDVI value during a 15-day compositing period. The NDVI is expressed on a scale between −1 and +1. GIMMS NDVI values range between −0.2 and 0.1 for snow, inland water bodies, deserts, and exposed soils, and increases from approximately 0.1–0.7 for increasing amounts of vegetation. The GIMMS dataset includes calibration using desert targets, atmospheric correction for stratospheric aerosol, and normalization for temporal changes in solar zenith angle [21].

2.2.2. Landsat Imagery

We used Landsat TM and ETM+ data to make a comparison with GIMMS NDVI due to the relatively higher spatial and spectral resolution of the sensors. The spatial resolution of 30 m was adequate to respond within stand changes, and the scene extent was large enough to cover the whole burned on two images. Moreover, since Landsat TM data are available for such an old fire event occurred on 1987. The Landsat TM and ETM+ data used in this study are list in Table1.

Table 1. Landsat TM and ETM+ scenes used in this analysis.

Year	Date	Sensor	Path/Row
1986	5 June	TM	121/23
1987	24 June	TM	121/23
1987	15 June	TM	121/22
2000	19 June	ETM+	121/23
2004	22 June	TM	121/23

2.3. Method

2.3.1. Mapping Fire Damage

In the present study, the difference in vegetation activity obtained from the NDVI between the pre- and post-fire periods was used to estimate fire damage. Fire damage represents the reflectance changes between the pre-fire vegetation and post-fire burn scar that can be interpreted as the extent of degradation of the pre-fire vegetation community. Therefore, fire damage (D) can be measured as a difference between pre- and post-fire NDVI values, as given by

$$D = NDVI_{pre-fire} - NDVI_0 \tag{1}$$

where $NDVI_{pre-fire}$ is the average NDVI value in the pre-fire period, *i.e.*, from 1984 to 1986, while $NDVI_0$ is the NDVI value in the fire year, *i.e.*, 1987. In this paper, we prefer fire damage to burn severity because the latter definition is often associated with numerous factors that include the effects on soil composition, the amount of organic material consumed by the fire, the effects on vegetation, e.g., amount of char on shrubs, scorch height and crown scorch, tree mortality or the presence of colonizers [22].

2.3.2. Modeling of Vegetation Recovery

Fire disturbances cause abrupt changes in the trend and seasonality of vegetation growth trajectories. Several studies concerning the regeneration of vegetation have proven that the NDVI is particularly useful for monitoring plant regrowth after fire disturbances [23–25]. To ascertain how long it takes burnt vegetation stands to return to their pre-fire average NDVI conditions, a relationship between pre- and post-fire NDVI values for a control scenario is necessary. The post-fire recovery also relies on the so-called healthy state [26]. Here, the healthy state is considered the theoretical potential vegetation attainable ($NDVI_{potential}$) by an ideal healthy state without any disturbance. Therefore, we define the stand regrowth index (SRI) at time *t* after the fire as

$$SRI_t = \frac{NDVI_{post,t}}{NDVI_{potential}} \times 100\% \tag{2}$$

where *t* is the elapsed year since the fire and $NDVI_{post,t}$ is the stand average annual NDVI at time *t*. Moreover, $NDVI_{potential}$ is the NDVI value of the healthy state, which is defined by the maximum NDVI value of the pre-fire period (1984–1986). Actually, it is very difficult or even impossible for all post-fire pixels to reach the healthy state. Therefore, stand regrowth index approaches 100% as time progresses following a fire disturbance. However, the rate never attains this value. Therefore, the growth rate can be used as a proxy for the vegetation recovery trend.

Furthermore, inter-annual NDVI signals are also greatly influenced by climate changes, e.g., temperature and precipitation anomalies. With the goal of separating the inter-annual variations caused by climate from changes in NDVI and highlighting fire-induced effects on vegetation, another similar index using a control stand NDVI instead of the pre-fire NDVI has been used in numerous fire recovery studies [9,27,28]. This relative regrowth index (RRI) at time *t* can be expressed as follows:

$$RRI_t = NDVI_{B,t} - NDVI_{C,t} \tag{3}$$

where $NDVI_{B,t}$ and $NDVI_{C,t}$ are the average NDVI values of the burned area and unburned control plot, respectively, derived from the GIMMS NDVI.

The advantage of using SRI to evaluate post-fire recovery is that it relates all post-fire NDVI values to the actual situation in the stand before the fire. However, pre-fire vegetation is specific to antecedent environmental conditions affecting vegetation growth. Hence, by utilizing an adjacent unburned control stand NDVI to derive the RRI, changes in environmental conditions are potentially captured by the NDVI signals throughout the analysis period [27]. It is very important for the calculation of the RRI that the selected control area has similar properties (e.g., vegetation type or climate) to the burnt area. The control area was required to have a long history without fire or other disturbances to ensure that it was not undergoing changes associated with vegetation recovery. To minimize differences in temperature and precipitation characteristics, the selected control area should have a similar elevation range to the burned area. In considering these premises, an adjacent area to the fire scar was chosen as the unburned control area (Figure 1).

2.3.3. Mann-Kendall Trend Assessment

Trend significance was evaluated using a statistical rank-based nonparametric Mann-Kendall test [29,30], which is a commonly used method to assess the significance of monotonic trends in long-term time series. It has the advantage of not assuming any distributional form for the data and has similar capabilities as its parametric counterparts. In this study, the time series of the calculated *SRI*s are analyzed to identify meaningful long-term trends using the Mann-Kendall statistics. In the Mann-Kendall test, the data are ranked with reference to time; each data point is treated as the reference for the data points in successive time periods [31]. The equation used to calculate the Mann-Kendall correlation coefficient (S) is defined by Kendall as

$$S = \sum_{i=1}^{n-1} \sum_{j=i+1}^{n} sign\left(SRI_i - SRI_j\right) \tag{4}$$

where

$$sign\left(SRI_i - SRI_j\right) = \begin{cases} 1 & if \ \ SRI_i - SRI_j < 0 \\ 0 & if \ \ SRI_i - SRI_j = 0 \\ -1 & if \ \ SRI_i - SRI_j > 0 \end{cases} \tag{5}$$

Here, *n* is the length of the time series dataset and SRI_i and SRI_j are the observational stand regrowth index at times *i* and *j*, respectively. According to Mann and Kendall, the statistic S is approximately normal when $n \geq 8$ with the mean and the variance as follows:

$$E\,(S) = 0 \tag{6}$$

$$\text{Var(S)} = \frac{n(n-1)(2n+5) - \sum_{i-1}^{n} t_i(i)(i-1)(2i+5)}{18} \tag{7}$$

where t_i denotes the number of ties of extent *i*.

The equation used to calculate Mann-Kendall significance (U and p) is as follows:

$$U = \begin{cases} \dfrac{S-1}{\sqrt{\text{Var(S)}}} & \text{for} \quad S > 0 \\ 0 & \text{for} \quad S = 0 \\ \dfrac{S+1}{\sqrt{\text{Var(S)}}} & \text{for} \quad S < 0 \end{cases} \tag{8}$$

The U statistic follows the standard normal distribution with zero mean and unit variance under the null hypothesis of no trend. A positive U value indicates an upward trend; a negative value indicates a downward trend. The *p* value of an MK statistic *S* can then be determined using the normal cumulative distribution function

$$p = 2[1 - \emptyset(|U|)] \tag{9}$$

where $\emptyset(|U|)$ denotes the cumulative distribution function of a standard normal vitiate.

3. Results and Discussion

3.1. Fire Damage Assessment

The goal of this study was to examine the spatial and temporal patterns of forest regeneration and then assess the driving factors relevant to the vegetation recovery process, especially for fire damage. The differences between the immediate post-fire and pre-fire NDVI values enabled us to identify the fire-damaged areas that were likely burned. Figure 2 shows a spatial pattern of fire damage that was computed from the pre- to post-fire difference in GIMMS NDVI. Red pixels represent large NDVI differences between pre- and post-fire, while blue pixels represent small NDVI differences. Fire damage is expected to influence the spatial configuration and arrangement of forest patches, contributing to and influencing ecological processes during post-fire recovery and succession [32]. Therefore, to track vegetation behavior that was affected by different fire damage extents, we classified the fire damage into five classes using the z-score (standard deviation) method [33].

A z-score, or standard deviation, measures the dispersion of data. A reclassification procedure was used to divide the z-scores of the simple difference images (the standardized difference between pre- and post-fire NDVI values) into five categories (Table 2).

Figures 3 and 4 illustrate the result of the fire damage classification using the z-score approach. The image is mapped in a blue-red color scale. Low z-scores are represented in blue, while a red color was assigned to high z-score pixels. The spatial pattern of the fire damage classes is clearly visible in the map with an evident differentiation between very high and slight patches.

There were five different fire sources for this large fire event. Some burned areas joined together while others did not (Figure 4 and Table 3). Therefore, very high and high fire damage pixels were concentrated in a few disjunctive regions.

Figure 2. Fire damage map of the study area for the Daxing'anling fire event with fire damage values obtained using Equation (1).
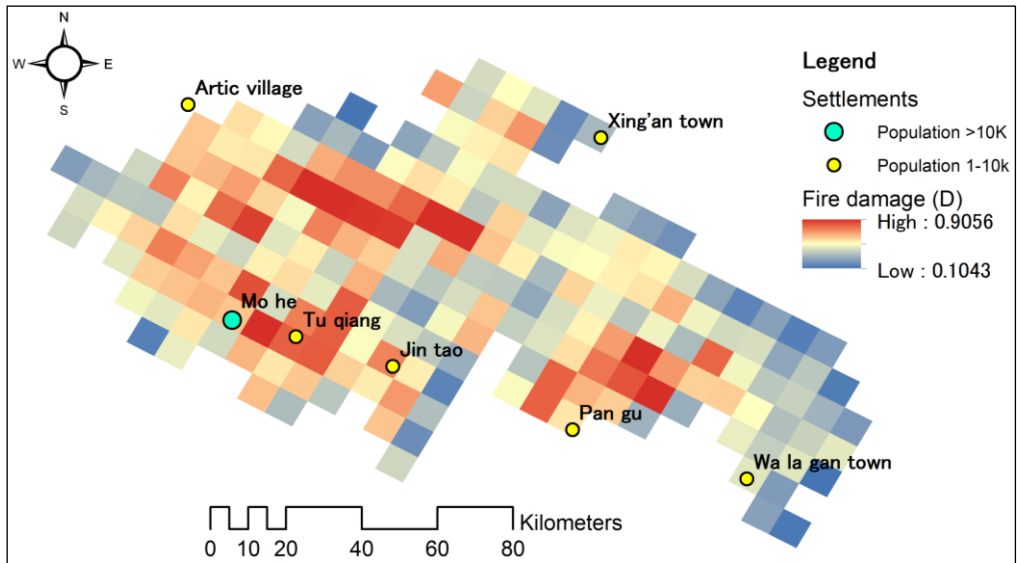

Table 2. Fire damage classification using the z-score method.

Pre-Fire Year (1984–1986)	Post-Fire Year (1987)	Standard Difference	z-Score	Fire Damage Class	Pixels	Percentage (%)
0.7708	0.6542	−2~−1	1	Slight	5	2.44%
0.7764	0.5352	−1~0	2	Low	49	23.90%
0.7852	0.3868	0~1	3	Medium	94	45.85%
0.7884	0.2239	1~2	4	High	46	22.44%
0.8165	0.0524	2~999	5	Very high	11	5.37%

Figure 3. The fire damage of the entire burned area divided into five classes: Very high (VH), High (H), Moderate (M), Low (L) and Slight (S).
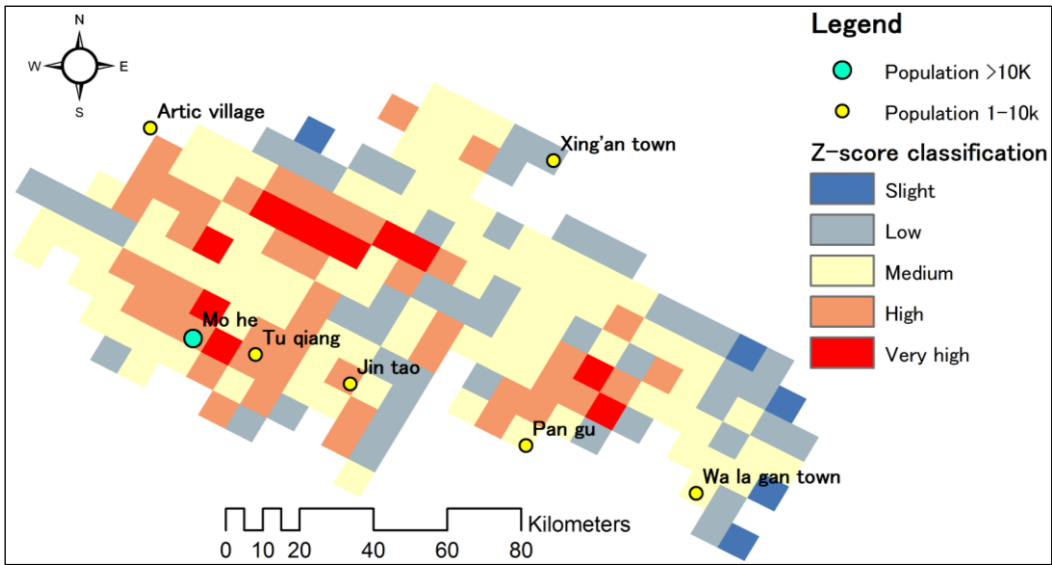
Figure 4. Fire sources and fire damage classes: Very high (VH), High (H), Moderate (M), Low (L) and Slight (S). The base map image is a composition of two Landsat 5 TM images from June 1987 (false color composite bands: red-band 7; green-band 4; blue-band 1). Beryl green grids were chose to track the detail vegetation signals using Landsat images with 30 m spatial resolution.
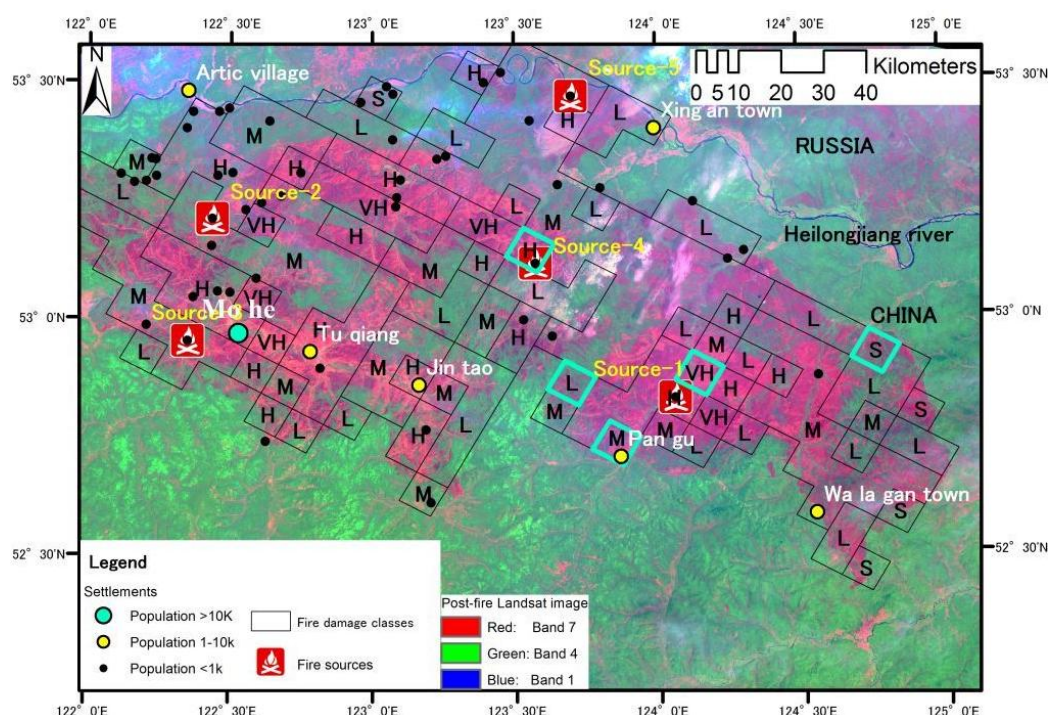

Table 3. Five sources of the 1987 large fire related to Figure 4.

| Fire Source	Name	Longitude	Latitude	Burned Area	Ignition Reason
Source-1	Gulian	122°22'	52°26'	38×10^4 ha	Electric spark
Source-2	Hewan	122°21'	53°11'	33.8×10^4 ha	Smoking
Source-3	Pangu	123°43'	52°45'	28×10^4 ha	Unknown
Source-4	Xingan	122°22'	122°22'	616 ha	Smoking
Source-5	Yixi	123°25'	53°05'	587 ha	Electric spark

3.2. Temporal Analysis of Post-Fire Vegetation Trajectory

3.2.1. Monthly Dynamics of Post-Fire Vegetation Trajectory

The relationship between pre-fire (1986) and fire year (1987) NDVI values is illustrated in a series of scatter plots (Figure 5). The location of the cloud of points shows a large shift away from the 1:1 line when the fire occurred in May and a positive recovery trend after the fire. From January to April (Figure 5a–d), the cloud of points is close to the 1:1 line, which indicates the NDVI values were generally equal during periods without fire disturbances in both years. However, Figure 5e shows that there was a sharp decrease when the fire occurred in May 1987. Following the fire event, there was a rapid increase from June to August (Figure 5f–h), which was likely the NDVI response of the understory vegetation (e.g., herbaceous and shrubs) to temperature or precipitation variability [34,35]. From September to November, the Great Xing'an Mountain entered autumn; NDVI values decreased in both

years with the spread of colored foliage and the percentage of fallen leaves increasing. Regardless, Figure 5j also shows clear NDVI departures when post- and pre-fire conditions are compared. This is because colored leaves fall from grasses and shrubs while the tree leaves remain green in October. The difference in NDVI values appeared again in this month. Therefore, October was a better than the others to distinguish post- and pre-fire vegetation conditions using NDVI signals. Thereafter, this region was covered by snow from December to the following February. During this period, it is difficult to find evidence of fire effects on vegetation from NDVI values due to the values reaching a minimum for the entire seasonal cycle.

Figure 5. Monthly scatterplots of post-fire normalized difference vegetation index (NDVI) (1987) *versus* pre-fire NDVI (1986) ((**a**) January, (**b**) February, (**c**) March, (**d**) April, (**e**) May, (**f**) June, (**g**) July, (**h**) August, (**i**) September, (**j**) October, (**k**) November, (**l**) December) for the large fire on May 1987.
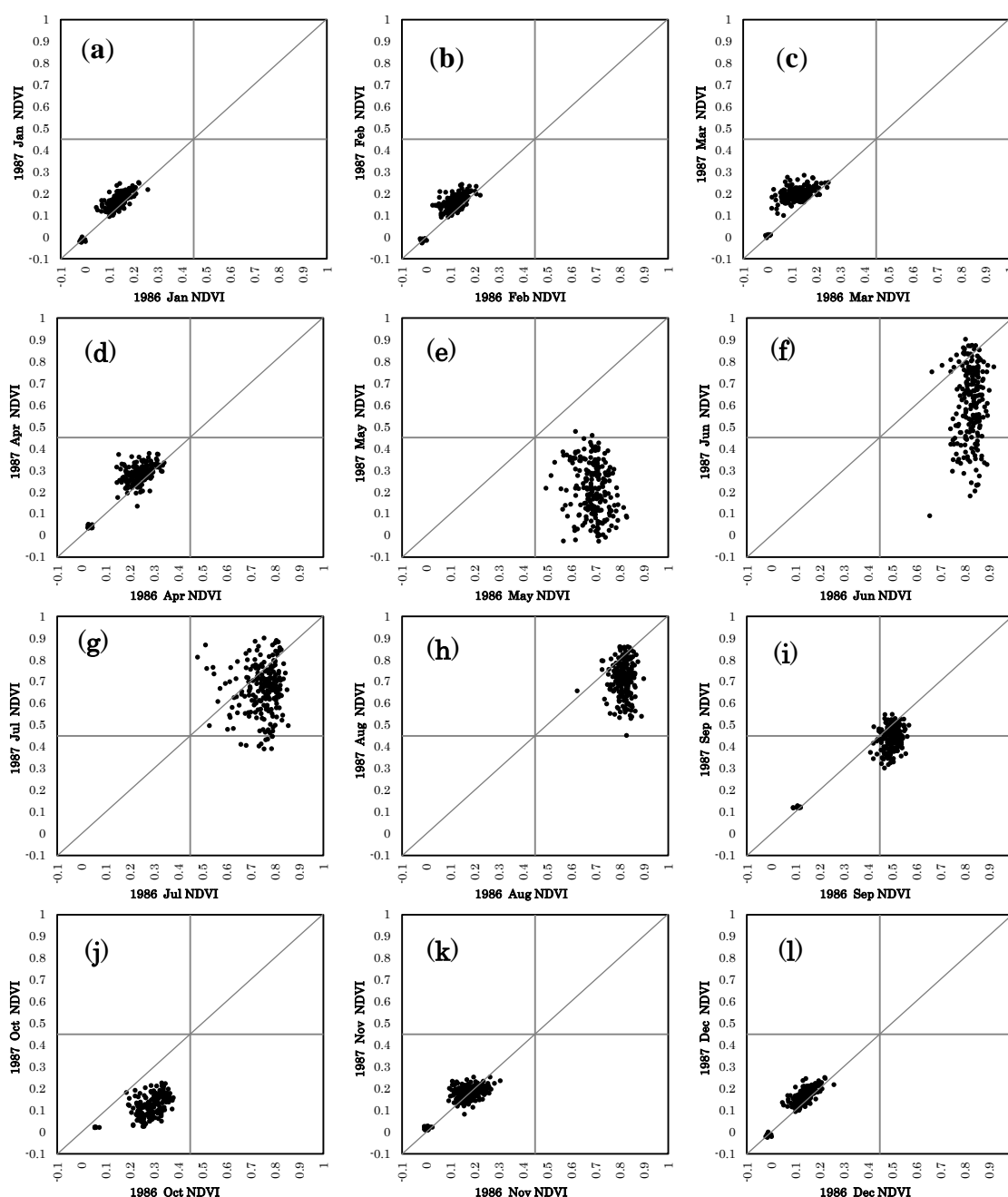
Shortly after the fire event, the NDVI signal should decrease significantly due to the disappearance of green grasses and shrubs before rapidly increasing again in the following months because of the re-growth of understory vegetation occurs and the phenology trajectory effect. Therefore, to avoid the phenology effect we further compared monthly NDVI trajectories of the normal year (without fire) and fire year (Figure 6). The trajectory of black points (average NDVI values for each month) is expected to be distributed along the 1:1 line when there is no disturbance; the monthly differences between the two normal years are very small (Figure 6a). However, for the fire year, there was a large increase in the fire month (May); most points following the fire are below the 1:1 line, indicating a pronounced decrease in greenness due to the fire.

Figure 6. Monthly NDVI trajectories of (**a**) a normal year and (**b**) the fire year. The points within the green box represent the growing season (April to October), while the points within the black box represent the snow cover season (November to March). The red point represents the month that the fire occurred.

(**a**)   (**b**)
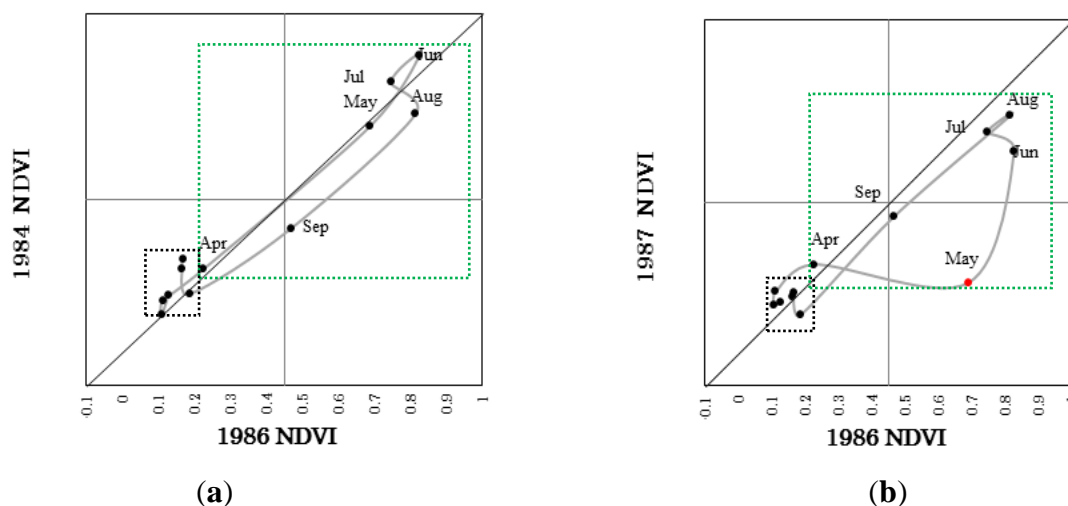
3.2.2. Yearly Dynamics of Post-Fire Vegetation

The entire study period (1984–2006) includes three parts: pre-fire years (1984–1986), fire event year (1987) and post-fire years (1988–2006). Figure 7 shows the evolution of RRI, which was calculated using NDVI differences between fire scars and unburned control areas for the growing season average (April to October) and June (the month right after the fire in 1987) time series. Zero on the time scale represents the burn year, *i.e.*, relative year 0 was the year of the wildfire event. Relative year −1 and +1 were years immediately before and after the fire event, respectively. In both series, there was an abrupt decrease in RRI values from 0 to −0.1 and −0.25 for the growing season average and June, respectively. Both series had low temporal variability in the pre-fire period that progressively increased in the post-fire period.

The June series RRI values decreased abruptly after the Daxing'anling fire in 1987. This decrease was larger than for the growing season average time series. The RRI underwent a progressive increase during the first four years following the fire. Different recovery trends have been explained in relation to the species types installed and the biophysical constraints of the sites [23]. Generally, understory grass can recover to very high RRI values within several months following a fire. Dwarf shrubs also exhibit

rapid regrowth capabilities, which can reach the saturating biomass stage within a short time scale (3–5 years). Therefore, the increase in this phase was mainly the result of survived dwarf shrub and understory grass. There is a slight decrease in the relative year 5, which was mainly a consequence of post-fire logging and planning. The RRI value was less than 0 during the post-fire period. However, the recovery trend was well pronounced and the system tended to recover to pre-disturbance conditions. Figure 7 shows a good recovery at relative year 19 with RRI reaching zero, which indicates there was no difference between burn scar and control plot. However, to confirm this result over a much longer period, additional observations are required.

Figure 7. The evolution of RRI calculated using NDVI difference between fire scars and the unburned control area for the growing season average (April to October) and June (the month immediately after the fire in 1987) time series. Zero on the time scale represents the burn year, *i.e.*, relative year 0 is the year of the wildfire event. Relative year −1 and +1 corresponds to the year before and after the fire event, respectively.
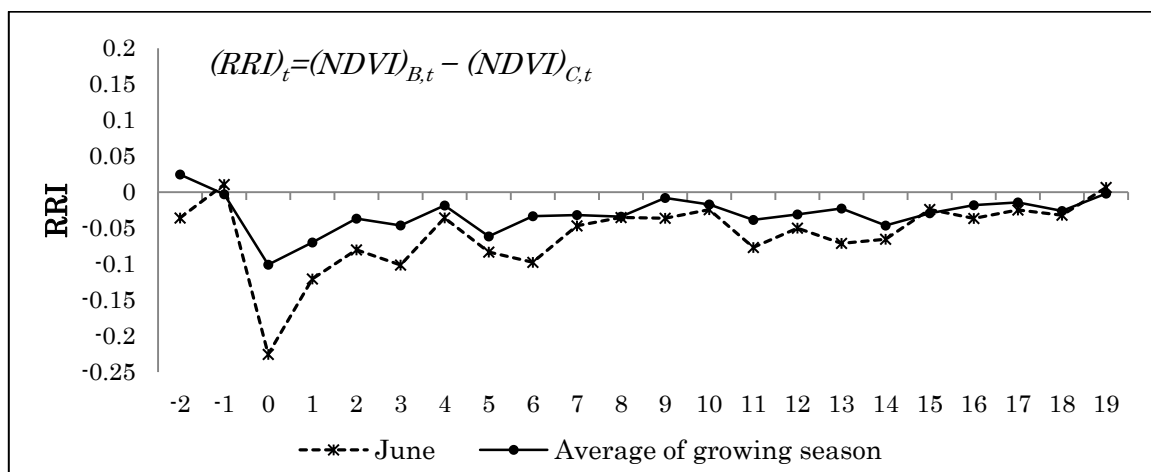
3.3. Spatial Pattern and Trend Analysis of Post-Fire Stands Regrowth Index (SRI)

An annual stands regrowth index (SRI) series was estimated from the vegetation response after the fire. Most of the burned pixels suggest that vegetation responses follow a positive trend, increasing their annual SRI responses in subsequent years (1988–2006) after this fire event (Figure 8). It is evident from the figure that substantial change occurred within this region from 1988 to 2006. There was a small annual increase in SRI values during the first five years following the fire. However, there was a more robust annual increase between years 10 and 19 in the subsequent period. This change in the rate was due to intensive salvage harvesting of standing dead logs in the first two years following the fire and then coniferous trees were planted to restore the timber volume of coniferous species because lumbering was the main forest industry in this region [36]. Figure 9 presents a significance image and degree of significance for the post-fire stands regrowth index (SRI) trend from the study area using the simple non-parametric Mann-Kendall test (single pixel-based analysis). The blue-green color shows the statistically significant positive trends. Most of the study area had significant increases in SRI, corroborating accounts of a general greening of the burned area during this period. A trend was considered statistically significant (at $P \leq 0.05$) when the Mann-Kendall (MK) statistics U was either

≥ 1.96 or ≤ −1.96 [29,30]. Therefore, the degree of significance of the post-fire stands regrowth index (SRI) trend using a non-parametric Mann-Kendall test can be divided into four categories: U < −1.96, significant downward trend; −1.96 ≤ U < 0, downward trend, however not significant; 0 ≤ U < 1.96, upward trend, however not significant; and 1.96 ≤ U, significant upward trend (Figure 9b). Table 4 demonstrates that all very high (VH) damage pixels had an upward trend; there was a significant upward trend (Mann-Kendal significance (U) ≥ 1.96) for 18% of the pixels and a non-significant upward trend for 82% of the pixels. Our results agree well with the findings of similar researches conducted by Wang and He *et al.* [17,37]. They found that larch abundance increases due to increasing planting intensity and the degree of increased abundance among these planting intensity scenarios is different. The results also suggest that approximately 65% and 61% of the high (H) and medium (M) fire damage pixels, respectively, underwent a non-significant upward trend. However, for the slight (S) and low (L) damage classes, this number was very low because tree planting mainly occurred in the severely burned area (approximately equal to the Medium, High and Very High fire damage areas combined). The main species planted was *L. gmelinii*, with a small area of *P. sylvestris* var. Mongolia and Korean Spruce (*Picea koraiensis*). Therefore, the severely burned area exhibited a better recovery trend than the lightly burned regions, similar to the results of Li *et al*. (2010). By 1997, approximately 50% of the severely burned area had been reforested, mostly in high accessibility areas and locations with good site conditions. In the moderately burned areas (30%−70% of trees dead), human promoted restoration was conducted with mechanical plows. However, in the lightly burned areas (less than 30% of trees dead), natural regeneration was permitted to occur [36]. Additionally, Wang and He *et al*. believed that spatial pattern of plantation also influences the three species, with higher larch and pine abundance and lower white birch abundance under dispersed planting than that under aggregated planting [37].

Table 4. The degree of significance for the post-fire stands regrowth index (SRI) trends using a non-parametric Mann-Kendall test.

Fire Damage Class		Mann-Kendal Significance (U)			
		U < −1.96	−1.96 ≤ U < 0	0 ≤ U < 1.96	1.96 ≤ U
		Significant Downward Trend	Downward Trend, However Not Significant	Upward Trend, However Not Significant	Significant Upward Trend
Slight	Pixel counts	0	2	3	0
(S)	Percentage (%)	0%	40%	60%	0%
Low	Pixel counts	3	33	12	1
(L)	Percentage (%)	6%	67%	24%	2%
Medium	Pixel counts	3	32	57	2
(M)	Percentage (%)	3%	34%	61%	2%
High	Pixel counts	0	13	30	3
(H)	Percentage (%)	0%	28%	65%	7%
Very High	Pixel counts	0	0	9	2
(VH)	Percentage (%)	0%	0%	82%	18%

Figure 8. The trajectory of the post-fire stands regrowth index (SRI) for the relative year 1, 5, 10, 15 and 19.
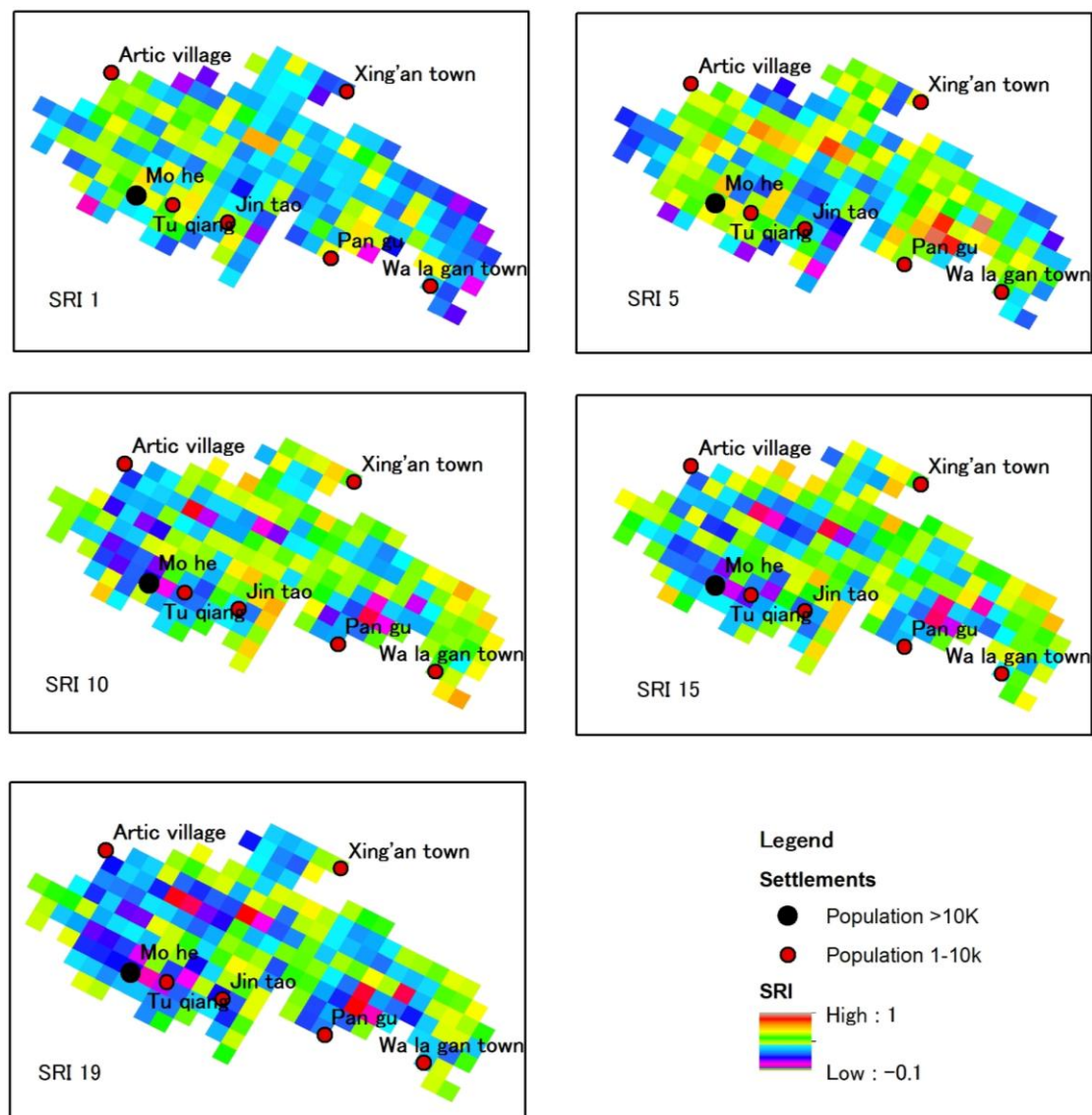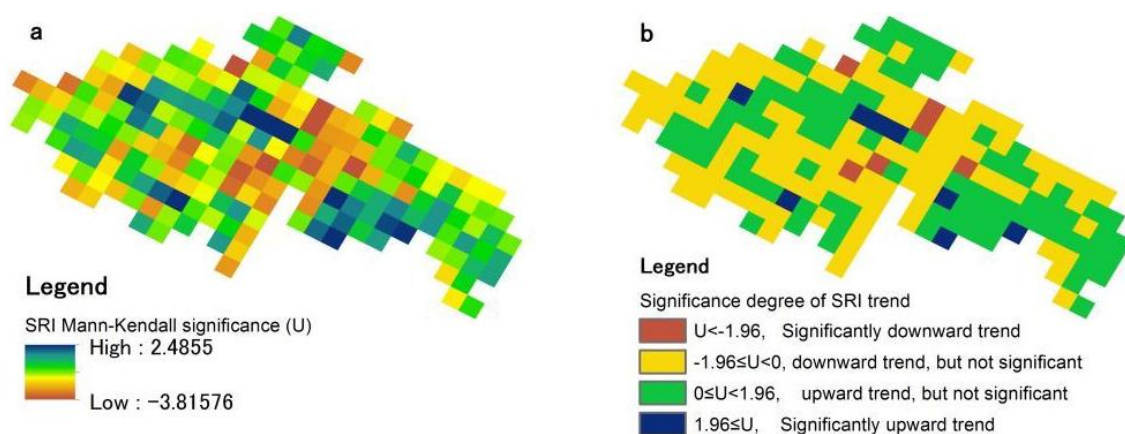

Figure 9. (**a**) The stands regrowth index (SRI) significance distribution using a non-parametric Mann-Kendall test and (**b**) the degree of significance degree for the post-fire stands regrowth index (SRI) trend using a non-parametric Mann-Kendall test.

3.4. Assessment against Landsat-NDVI

With higher spatial resolution than NOAA/AVHRR, enable the delineation of NDVI with a higher degree of accuracy. We attempted to assess the agreement of the GIMMS NDVI by comparing with NDVI extracted by Landsat TM/ETM+ sensors. We used Landsat TM and ETM+ data due to the relatively high spatial (30 m) and spectral resolution of the sensors. Moreover, Landsat TM data are available in the 1980s; the response of post-fire vegetation may be estimated using these data. Five 8 km × 8 km simples were acquired for the same location with GIMMS NDVI to track the detail vegetation signals in Landsat imagery (Figure 4). Landsat images were selected at close dates (5 June 1986, 15 June 1987, 19 June 2000 and 22 June 2004) in order to avoid the influences of phenological differences (Table 1 and Figure 10). To account for differences in the temporal resolution, GIMMS 15-day images nearest to the Landsat sample acquisition date were selected.

Figure 10. Landsat TM/ETM+ images (RGB:432) illustrating fire-caused changes on the ground vegetation. The locations of these five tracked simples can be found in Figure 4. Minus and plus signs represent pre-fire and post-fire period, respectively. Fire damage classes: Very High (VH); High (H); Moderate (M); Low (L); Slight (S).
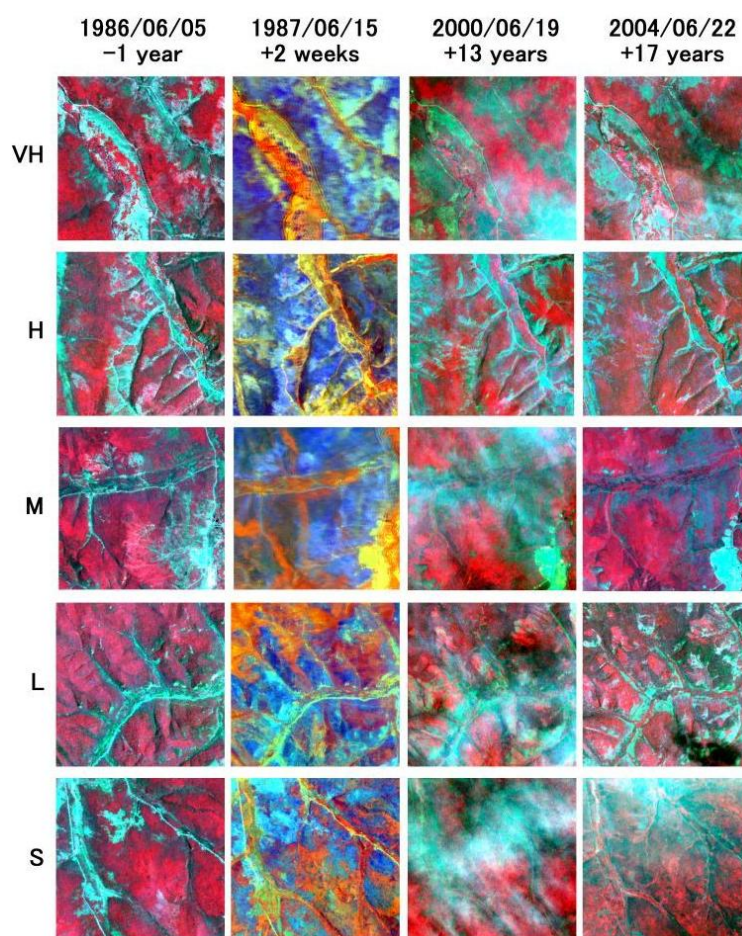

Figure 11 shows a similar the NDVI trends of GIMMS and Landsat. GIMMS dataset appears positively biased compared to Landsat-NDVI values. Landsat-NDVI values confirm that the GIMMS dataset overestimates NDVI in this region, which is likely due to GIMMS NDVI consisting primarily of

maximum acquisitions. A stronger regrowth trend of very high fire damage areas was found in both GIMMS and Landsat-NDVI. It indicates that tree planting in very high fire damage areas plays a positive role in the recovery process.

Figure 11. Comparison GIMMS NDVI (**left**) with Landsat NDVI (**right**).
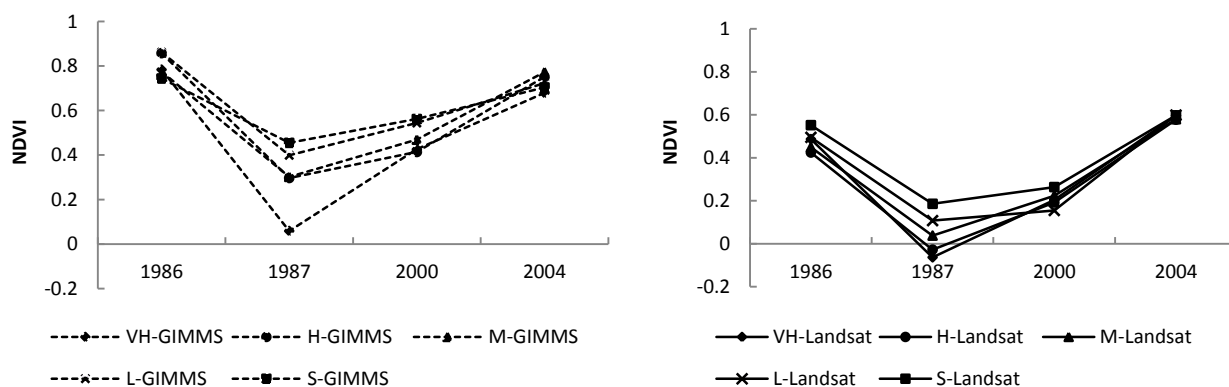
NDVI is an indicator of vegetation cover density and plant growth condition [38]. Pixel greenness is interpreted as indicating the presence of vegetation chlorophyll. Thus, NDVI can be interpreted originally as a proxy of "green leaf biomass", based on experience mainly with crops, grasslands and forest. As an example of the potential usefulness of the NDVI, Tucker *et al*. constructed monthly greenness images for Africa in 1981 and 1982 which graphically show the advance and retreat of the tropical summer wet season and year-to-year differences in surface greenness, which they interpreted as primary production [39–41]. Maxim *et al*. presented a simple modification to an existing empirical NDVI-based model for biomass estimation, using the ratio between the mean annual precipitation and a threshold rain level representing the transition from dwarf-shrub to shrub dominance [42]. H. Janin *et al*. assessed the performance of NDVI as a proxy for plant biomass, which reinforces the idea that NDVI is most often a nonlinear proxy of plant biomass [43]. Although, NDVI has been used to estimate vegetation biomass in many ways, it is also limited due to saturation of value in dense vegetation. Therefore, to better understand the biomass recovery in post-fire area, multiple sources remote sensing data (such as, leaf area index (LAI), GPP, NPP and SAR data) should be considered in the future study. For this study, the whole burned area was treated as a protection zone after the fire. Nobody can enter into this region without an official permission. Only helpful planting actions were taken to restore the timber volume without any other negative human disturbances during recent two decades. Thus, in this case, we believe that the NDVI signal is closely and positive correlated with forest biomass. Although, the GMMIS resolution is not high, the temporal trend of stands regrowth index (SRI) also can reflect the long-term vegetation response after the fire (Figures 8 and 9).

4. Conclusion

This paper described the long-term effects on vegetation of a catastrophic fire on the northern Great Xing'an Mountain in 1987 that were observed using a nonparametric Mann-Kendall (MK) statistics method and analyzing the AVHRR GIMMS 15-day composite NDVI dataset. Both temporal and spatial characteristics were analyzed under natural regeneration and tree planting scenarios from 1984 to 2006.

Regressing post-fire NDVI values on pre-fire values helped identify the NDVI for completely burned pixels in vegetation stands; this value was subsequently used in an index to quantify stand differences in fire damage. October was established as a better month compared with the other months to distinguish the post- and pre-fire vegetation conditions using NDVI signals because grasses and shrubs lose their colored leaves, while the leaves on healthy trees remain green. The Mann-Kendall (MK) statistics method is capable of detecting vegetation trends in relatively long time series. Normally, high fire damage area performs a slower and even harder regrowth progress than medium burned area under natural recovery conditions without tree planting. However, because tree planting primarily occurred in the severely burned areas (approximately equal to the Medium, High and Very High fire damage areas combined), this region exhibited a better recovery trend than the lightly burned locations (Table 4). Reasonable tree planting can substantially quicken the recovery process and shorten the restoration time of target species. We believe that it is necessary to incorporate information about spatial patterns of plantation into planting strategies. This research involves a large area (1.33×10^6 hm^2) and a long time span (1984–2006). Therefore, it is unfeasible to perform real field validation for such a study. More detailed satellite analyses and field data are required in the future for a more convincing validation of the results.

Acknowledgments

Conflicts of Interest

The authors declare no conflict of interest.

Reference

1. Beck, P.S.A.; Goetz, S.J.; Mack, M.C.; Alexander, H.D.; Jin, Y.; Randerson, J.T.; Loranty, M.M. The impacts and implications of an intensifying fire regime on Alaskan boreal forest composition and albedo. *Glob. Chang. Biol.* **2011**, *17*, 2853–2866.
2. Wulder, M.A.; White, J.C.; Alvarez, F.; Han, T.; Rogan, J.; Hawkes, B. Characterizing boreal forest wildfire with multi-temporal Landsat and Lidar data. *Remote Sens. Environ.* **2009**, *113*, 1540–1555.
3. Kang, S.; Kimball, J.S.; Running, S.W. Simulating effects of fire disturbance and climate change on boreal forest productivity and evapotranspiration. *Sci. Total Environ.* **2006**, *362*, 85–102.
4. Cahoon, D.R.; Stocks, B.J.; Levine, J.S.; Cofer, W.R.; Pierson, J.M. Satellite analysis of the severe 1987 forest fires in northern China and southeastern Siberia. *J. Geophys. Res.*: *Atmos.* **1994**, *99*, 18627–18638.
5. Tan, K.; Piao, S.; Peng, C.; Fang, J. Satellite-based estimation of biomass carbon stocks for northeast China's forests between 1982 and 1999. *For. Ecol. Manag.* **2007**, *240*, 114–121.

6. Fang, J.; Chen, A.; Peng, C.; Zhao, S.; Ci, L. Changes in forest biomass carbon storage in China between 1949 and 1998. *Science* **2001**, *292*, 2320–2322.

7. Zhong, M.; Fan, W.; Liu, T.; Li, P. Statistical analysis on current status of China forest fire safety. *Fire Saf. J.* **2003**, *38*, 257–269.

8. Goetz, S.J.; Fiske, G.J.; Bunn, A.G. Using satellite time-series data sets to analyze fire disturbance and forest recovery across Canada. *Remote Sens. Environ.* **2006**, *101*, 352–365.

9. Cuevas-GonzÁLez, M.; Gerard, F.; Balzter, H.; RiaÑO, D. Analysing forest recovery after wildfire disturbance in boreal Siberia using remotely sensed vegetation indices. *Glob. Chang. Biol.* **2009**, *15*, 561–577.

10. Matthews, S.; Sullivan, A.; Gould, J.; Hurley, R.; Ellis, P.; Larmour, J. Field evaluation of two image-based wildland fire detection systems. *Fire Saf. J.* **2012**, *47*, 54–61.

11. Segah, H.; Tani, H.; Hirano, T. Detection of fire impact and vegetation recovery over tropical peat swamp forest by satellite data and ground-based NDVI instrument. *Int. J. Remote Sens.* **2010**, *31*, 5297–5314.

12. Parsons, A. *Burned Area Emergency Rehabilitation Soil Burn Severity Definitions and Mapping Guidelines Draft*; USDA Forest Service, Rocky Mountain Research Station: Missoula, MT, USA, 2003.

13. Balzter, H.; Gonzalez, M.C.; Gerard, F.; Riaño, D. Post-Fire Vegetation Phenology in Siberian Burn Scars. In Proceedings of 2007 IEEE International Geoscience and Remote Sensing Symposium, Barcelona, Spain, 23–28 July 2007; pp. 4652–4655.

14. Telesca, L.; Lasaponara, R. Pre- and post-fire behavioral trends revealed in satellite NDVI time series. *Geophys. Res. Lett.* **2006**, *33*, doi: 10.1029/2006GL026630.

15. Leon, J.R.R.; van Leeuwen, W.J.D.; Casady, G.M. Using MODIS-NDVI for the modeling of post-wildfire vegetation response as a function of environmental conditions and pre-fire restoration treatments. *Remote Sens.* **2012**, *4*, 598–621.

16. Zhou, L.M.; Tucker, C.J.; Kaufmann, R.K.; Slayback, D.; Shabanov, N.V.; Myneni, R.B. Variations in northern vegetation activity inferred from satellite data of vegetation index during 1981 to 1999. *J. Geophys. Res.*: *Atmos.* **2001**, *106*, 20069–20083.

17. Wang, X.; He, H.S.; Li, X. The long-term effects of fire suppression and reforestation on a forest landscape in Northeastern China after a catastrophic wildfire. *Landsc. Urban Plan.* **2007**, *79*, 84–95.

18. Wu, Z.W.; He, H.S.; Chang, Y.; Liu, Z.H.; Chen, H.W. Development of customized fire behavior fuel models for boreal forests of northeastern China. *Environ. Manag.* **2011**, *48*, 1148–1157.

19. Turner, M.G.; Romme, W.H.; Gardner, R.H.; Hargrove, W.W. Effects of fire size and pattern on early succession in Yellowstone National Park. *Ecol. Monogr.* **1997**, *67*, 411–433.

20. Li, X.; He, H.S.; Wu, Z.; Liang, Y.; Schneiderman, J.E. Comparing effects of climate warming, fire, and timber harvesting on a boreal forest landscape in northeastern China. *PLoS One* **2013**, *8*, e59747.

21. Pouliot, D.; Latifovic, R.; Olthof, I. Trends in vegetation NDVI from 1 km AVHRR data over Canada for the period 1985–2006. *Int. J. Remote Sens.* **2009**, *30*, 149–168.

22. Bastos, A.; Gouveia, C.M.; DaCamara, C.C.; Trigo, R.M. Modelling post-fire vegetation recovery in Portugal. *Biogeosciences* **2011**, *8*, 3593–3607.

23. Viedma, O.; Melia, J.; Segarra, D.; GarciaHaro, J. Modeling rates of ecosystem recovery after fires by using Landsat TM data. *Remote Sens. Environ.* **1997**, *61*, 383–398.

24. Van Leeuwen, W.J.D. Monitoring the effects of forest restoration treatments on post-fire vegetation recovery with MODIS multitemporal data. *Sensors* **2008**, *8*, 2017–2042.

25. Kennedy, R.E.; Yang, Z.; Cohen, W.B.; Pfaff, E.; Braaten, J.; Nelson, P. Spatial and temporal patterns of forest disturbance and regrowth within the area of the Northwest Forest Plan. *Remote Sens. Environ.* **2012**, *122*, 117–133.

26. Gouveia, C.; DaCamara, C.C.; Trigo, R.M. Post-fire vegetation recovery in Portugal based\newline on spot/vegetation data. *Nat. Hazard. Earth Syst. Sci.* **2010**, *10*, 673–684.

27. Hope, A.; Albers, N.; Bart, R. Characterizing post-fire recovery of fynbos vegetation in the Western Cape Region of South Africa using MODIS data. *Int. J. Remote Sens.* **2012**, *33*, 979–999.

28. Lampainen, J.; Kuuluvainen, T.; Wallenius, T.H.; Karjalainen, L.; Vanha-Majamaa, I. Long-term forest structure and regeneration after wildfire in Russian Karelia. *J. Veg. Sci.* **2004**, *15*, 245–256.

29. Mann, H.B. Nonparametric tests against trend. *Econometrica* **1945**, *13*, 245–259.

30. Kendall, M.G. *Rank Correlation Methods*; Griffin: London, UK, 1975.

31. Neeti, N.; Eastman, J.R. A contextual mann-kendall approach for the assessment of trend significance in image time series. *Trans. GIS* **2011**, *15*, 599–611.

32. Lee, S.-W.; Lee, M.-B.; Lee, Y.-G.; Won, M.-S.; Kim, J.-J.; Hong, S.-K. Relationship between landscape structure and burn severity at the landscape and class levels in Samchuck, South Korea. *For. Ecol. Manag.* **2009**, *258*, 1594–1604.

33. Nielsen, E.M.; Prince, S.D.; Koeln, G.T. Wetland change mapping for the US mid-Atlantic region using an outlier detection technique. *Remote Sens. Environ.* **2008**, *112*, 4061–4074.

34. Veraverbeke, S.; Gitas, I.; Katagis, T.; Polychronaki, A.; Somers, B.; Goossens, R. Assessing post-fire vegetation recovery using red-near infrared vegetation indices: Accounting for background and vegetation variability. *ISPRS J. Photogramm. Remote Sens.* **2012**, *68*, 28–39.

35. Pausas, J.G.; Bradstock, R.A.; Keith, D.A.; Keeley, J.E.; Network, G.F. Plant functional traits in relation to fire in crown-fire ecosystems. *Ecology* **2004**, *85*, 1085–1100.

36. Li, X.; He, H.; Wang, X.; Xie, F.; Hu, Y.; Li, Y. Tree planting: How fast can it accelerate post-fire forest restoration?—A case study in Northern Da Hinggan Mountains, China. *Chin. Geogr. Sci.* **2010**, *20*, 481–490.

37. Wang, X.; He, H.S.; Li, X.; Chang, Y.; Hu, Y.; Xu, C.; Bu, R.; Xie, F. Simulating the effects of reforestation on a large catastrophic fire burned landscape in Northeastern China. *For. Ecol. Manag.* **2006**, *225*, 82–93.

38. Wang, J.; Meng, J.J.; Cai, Y.L. Assessing vegetation dynamics impacted by climate change in the southwestern karst region of China with AVHRR NDVI and AVHRR NPP time-series. *Environ. Geol.* **2008**, *54*, 1185–1195.

39. Tucker, C.J.; Pinzon, J.E.; Brown, M.E.; Slayback, D.A.; Pak, E.W.; Mahoney, R.; Vermote, E.F.; El Saleous, N. An extended AVHRR 8-km NDVI dataset compatible with MODIS and SPOT vegetation NDVI data. *Int. J. Remote Sens.* **2005**, *26*, 4485–4498.

40. Fensholt, R.; Sandholt, I.; Stisen, S.; Tucker, C. Analysing NDVI for the African continent using the geostationary meteosat second generation SEVIRI sensor. *Remote Sens. Environ.* **2006**, *101*, 212–229.

41. Anyamba, A.; Tucker, C.J. Analysis of Sahelian vegetation dynamics using NOAA-AVHRR NDVI data from 1981–2003. *J. Arid Environ.* **2005**, *63*, 596–614.

42. Shoshany, M.; Karnibad, L. Mapping shrubland biomass along Mediterranean climatic gradients: The synergy of rainfall-based and NDVI-based models. *Int. J. Remote Sens.* **2011**, *32*, 9497–9508.

43. Santin-Janin, H.; Garel, M.; Chapuis, J.L.; Pontier, D. Assessing the performance of NDVI as a proxy for plant biomass using non-linear models: A case study on the Kerguelen archipelago. *Polar Biol.* **2009**, *32*, 861–871.